germs

MDPI

Article

Impact of Manganese Coordination and Cyclodextrin-Assisted Formulation on Thiabendazole Dissolution and Endothelial Cell Migration

Carmen-Ecaterina Leferman, Lacramioara Ochiuz, Laura Stoica, Liliana Georgeta Foia, Bogdan Minea, Cezar Ilie Foia, Victor Constantinescu, Oana Olariu, Alin Dumitru Ciubotaru * and Bogdan Alexandru Stoica

Grigore T. Popa University of Medicine and Pharmacy, 700115 Iasi, Romania; carmen-ecaterina.leferman@umfiasi.ro (C.-E.L.); lacramioara.ochiuz@umfiasi.ro (L.O.); laurastoica2004@yahoo.com (L.S.); georgeta.foia@umfiasi.ro (L.G.F.); bogdan-minea@umfiasi.ro (B.M.); foia.cezar-ilie@d.umfiasi.ro (C.I.F.); victor.constantinescu@umfiasi.ro (V.C.); oana-olariu@umfiasi.ro (O.O.); bogdan.stoica@umfiasi.ro (B.A.S.)

* Correspondence: alin-dumitru_ciubotaru@umfiasi.ro

Abstract

Background: Thiabendazole (TBZ), a benzimidazole with established antifungal and anthelmintic properties, has also been reported to exert antiangiogenic effects relevant to tissue remodeling and chronic inflammatory microenvironments. The present study examined how manganese coordination and cyclodextrin modify the dissolution behavior and endothelial activity of TBZ. Methods: Antiangiogenic potential was assessed through a human umbilical vein endothelial cells (HUVECs) scratch-wound migration assay. Dissolution profiles of TBZ, manganese–thiabendazole (MnTBZ), and MnTBZ/monochlorotriazynil-β-cyclodextrin (MCT-β-CD) formulation were evaluated under biorelevant pH conditions (1.2, 4.5, 6.8, 7.4) using the paddle method. Results: TBZ displayed a more rapid and extensive dissolution at pH 1.2, compared to MnTBZ. Partial dissociation at pH 4.5 modestly improved TBZ availability, while dissolution remained minimal at neutral pH. MCT-β-CD enhanced the solubility of MnTBZ at pH $\geq$ 6.8. In agreement with these profiles, TBZ exerted the strongest inhibition of endothelial migration, followed by MnTBZ/MCT-β-CD and MnTBZ. Conclusions: Manganese coordination and cyclodextrin formulation modulate both the dissolution behavior and endothelial migration-inhibitory activity of TBZ, suggesting that such formulation approaches may influence the delivery-related and functional properties of benzimidazole derivatives.

Keywords: thiabendazole; manganese complex; cyclodextrin; antiangiogenic activity; HUVEC scratch assay; benzimidazole derivatives; pH-dependent solubility; drug repurposing

Received: 19 November 2025
Revised: 10 December 2025
Accepted: 19 December 2025
Published: 22 December 2025

1. Introduction

The vascular system plays a fundamental role in maintaining tissue vitality by ensuring adequate oxygenation, nutrient supply, and metabolic balance. Its architecture develops through two complementary mechanisms: vasculogenesis, the de novo formation of vessels from endothelial progenitors, and angiogenesis, the growth and remodeling of existing vasculature through endothelial sprouting and migration [1,2]. Under physiological conditions, angiogenesis is tightly regulated and essential for development, wound healing, and tissue repair. However, when this regulation is lost, dysregulated neovascularization can

occur, contributing to disorders such as cancer, diabetic retinopathy, rheumatoid arthritis, and chronic inflammation [3,4].

A variety of antiangiogenic agents, including monoclonal antibodies (e.g., bevacizumab), small-molecule tyrosine kinase inhibitors (such as sunitinib, sorafenib, and axitinib), and endogenous inhibitors like endostatin and angiostatin, have been developed to suppress pathological neovascularization by targeting the vascular endothelial growth factor (VEGF) signaling pathway [5,6]. While these therapies have shown clinical benefit in several cancers and ocular diseases [7,8] their use may be limited by adverse effects, high costs, and reduced accessibility [9,10] prompting interest in alternative or complementary approaches [11].

In this context, drug repurposing—the identification of new uses for approved drugs—represents a pragmatic strategy, supported by known pharmacokinetics and established safety profiles [12,13] This approach also allows the exploration of compounds acting through non-classical angiogenic mechanisms, such as cytoskeletal remodeling or redox regulation [14,15].

Among repurposed pharmacological agents, thiabendazole (TBZ)—a benzimidazole derivative approved by the U.S. Food and Drug Administration in 1967 for antifungal and anthelmintic use—has emerged as an unexpected vascular disrupting agent with potent antiangiogenic activity [16]. Initially identified through evolutionary network analysis, TBZ was shown to inhibit endothelial cell proliferation, migration, and capillary morphogenesis, while also disassembling pre-existing vasculature in *Xenopus* sp. and mammalian models [17]. Remarkably, TBZ induces endothelial cell rounding and vessel regression without triggering apoptosis, and these effects are reversible upon drug withdrawal, consistent with a cytoskeletal mechanism of action [18,19].

Subsequent molecular studies revealed that TBZ acts primarily through interaction with β-tubulin, specifically targeting the TUBB8 isotype expressed in endothelial cells. By perturbing microtubule polymerization dynamics, TBZ destabilizes the endothelial cytoskeleton and inhibits angiogenic sprouting. This selective mechanism accounts for its strong vascular effects with minimal systemic toxicity [20]. Further optimization led to derivatives such as TBZ-07 and TBZ-19, which exhibit markedly enhanced potency against endothelial proliferation and tube formation [16]. Collectively, these findings identify TBZ and its derivatives as promising scaffolds for developing novel antiangiogenic and vascular-targeting agents.

A number of transition-metal coordination compounds have shown antiangiogenic effects by influencing endothelial signaling, oxidative stress, and vessel formation. For instance, Ru(III) complexes such as NAMI-A and KP1339 inhibit VEGF- and nitric-oxide-mediated endothelial migration and microvessel growth [21], while Zn(II) and Cu(II) complexes of benzimidazole ligands exhibit higher cytotoxic and antiangiogenic activity compared with their free ligands [22,23].

In this context, manganese complexes are of interest due to their biocompatibility and redox activity, which may support oxidative modulation and metabolic stability [24]. These properties provide a rationale for exploring manganese–thiabendazole (MnTBZ) complexes as potential modulators of TBZ's biological behavior. In addition, metal coordination can influence key biopharmaceutical parameters such as solubility and release kinetics [25]. Given the poor aqueous solubility of TBZ, such modifications may have a relevant impact on its biological performance [26].

In contrast, cyclodextrins (CD) can counteract the solubility limitations imposed by coordination stability by forming inclusion complexes that enhance apparent aqueous solubility and prevent drug precipitation [27–30]. This strategy has been successfully applied to benzimidazoles such as TBZ and albendazole, improving their dissolution and

bioavailability [31,32]. Thus, metal coordination and CD inclusion represent complementary approaches capable of modulating TBZ's release profile—from delayed release in the case of stable complexes to accelerated dissolution when inclusion complexes dominate the equilibrium [33–35].

In the present study, we reproduced the synthesis of the MnTBZ complex according to previously described procedures [36] and conducted a comparative evaluation of its dissolution profile relative to the parent drug and to a formulation with monochlorotriazynil-β-cyclodextrin (MCT-β-CD). In parallel, the scratch wound assay was employed using human umbilical vein endothelial cells (HUVEC) to assess whether Mn complexation influences TBZ's ability to modulate endothelial cell migration, a critical step in angiogenesis. In this regard, these experiments aim to provide preliminary insight into how manganese coordination may alter both the solubility and biological activity of TBZ, contributing to a deeper understanding of metal complexation as a tool for optimizing the pharmacological behavior of repurposed drugs.

2. Materials and Methods

2.1. Chemicals and Reagents

Thiabendazole ≥ 98% purity (Figure 1a) was purchased from Sigma-Aldrich/Merck (St. Louis, MO, USA) and used without further purification. The manganese–thiabendazole complex (MnTBZ), corresponding to the composition $[Mn(TBZ)(TBZH)(CH_3COO)]\cdot 0.5H_2O$, was prepared according to the procedure previously described [36]. Briefly, $Mn(CH_3COO)_2\cdot 4H_2O$ (0.5 g, 2.04 mmol) was dissolved in ethanol (100 mL) and reacted under reflux for 3 h with TBZ (0.82 g, 4.08 mmol). The resulting off-white solid was filtered, washed with ethanol and water, and air-dried (yield: 52%). The product's insolubility in water, ethanol, methanol, acetone, and DMSO is consistent with literature reports, and our study follows the structural information established in previous spectroscopic and analytical investigations [36].

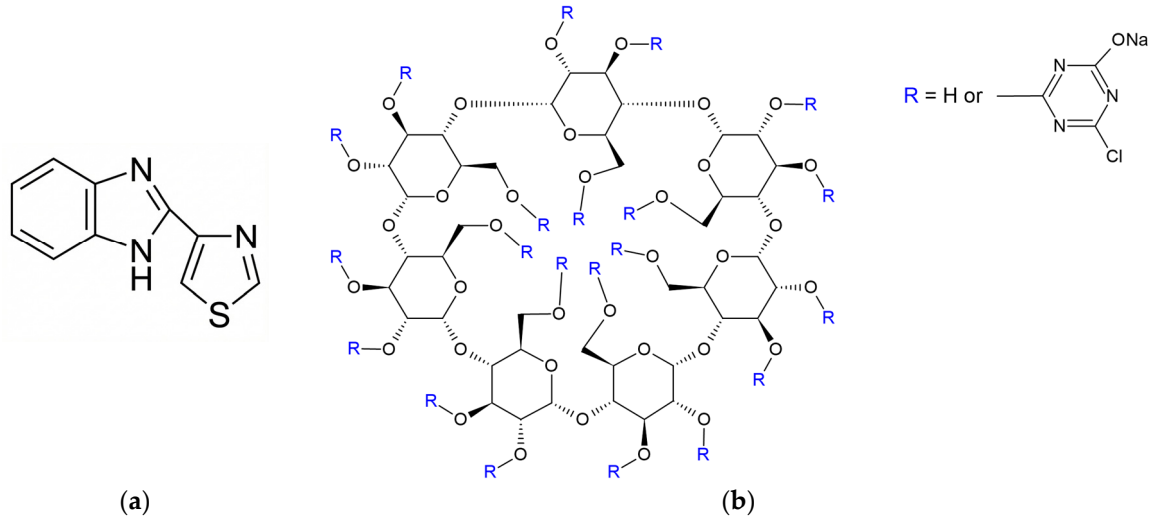

Figure 1. The structures of thiabendazole (**a**) and MCT-β-CD (**b**).

Monochlorotriazynil-β-cyclodextrin ≥ 97% (Figure 1b) was obtained from Sigma-Aldrich and mixed with MnTBZ in a 1:1 molar ratio by manual trituration, followed by mechanical and ultrasound homogenization. All other solvents and reagents used for synthesis, dissolution studies, and cell experiments (HCl, sodium acetate, phosphate buffers, ethanol, DMSO, phosphate-buffered saline, cell culture media) were of analytical grade and purchased from Sigma-Aldrich or Merck. Ultrapure water (18.2 MΩ·cm) was prepared using a Milli-Q system (Millipore, Burlington, MA, USA).

2.2. Dissolution Studies

The intrinsic dissolution behavior of TBZ, MnTBZ, and a MnTBZ/MCT-β-CD formulation (MnTBZ–CD) was evaluated using a USP Apparatus II (paddle method; Hanson Research Vision G2 Classic 6, Hanson Research, Chatsworth, CA, USA). Dissolution testing was performed in 500 mL of medium at 37 ± 0.5 °C with paddle rotation at 60 rpm. Biorelevant media were used to simulate different regions of the gastrointestinal tract: 0.1 N HCl (pH 1.2, gastric environment), acetate buffer (pH 4.5, transition from stomach to duodenum), and phosphate buffers at pH 6.8 and 7.4 (small intestine and distal intestinal/physiological conditions). For each experiment, 110 mg of TBZ, MnTBZ, or a 1:1 molar MnTBZ/MCT-β-CD mixture were added to the dissolution vessel. The mass of each sample introduced into the dissolution vessel was normalized to contain the same TBZ-equivalent amount. Accordingly, the quantity of MnTBZ and MnTBZ/MCT-β-CD was calculated based on the TBZ content of the complex. Aliquots of 2 mL were withdrawn at predefined intervals (5, 10, 15, 30, 45, 60, 90, 120, 150, 180, 210, 240, 270, and 300 min), immediately filtered through 0.45 µm membranes to remove undissolved particles, and replaced with an equal volume of preheated medium to maintain constant volume and sink conditions.

MCT-β-CD was added to assess its ability to enhance the aqueous solubility and dissolution rate of MnTBZ, a well-established strategy for improving the performance of poorly water-soluble drugs. MCT-β-CD was selected for further studies based on preliminary screening experiments showing its superior ability to enhance the dissolution of MnTBZ compared to the other cyclodextrin derivatives tested.

The concentration of dissolved compound was determined by UV–VIS spectrophotometry at 298 nm [37], where both TBZ and MnTBZ exhibit maximum absorbance. Calibration curves were prepared in each medium to ensure accuracy (R^2 = 0.992–0.998; LOD = 0.0014–0.0031 mg/mL; LOQ = 0.0042–0.0093 mg/dL). Dissolution profiles were expressed as the percentage of drug dissolved versus time, and the influence of pH on dissolution kinetics was evaluated. All measurements were carried out in triplicate (n = 3), and results were expressed as mean ± standard deviation (SD).

2.3. Cell Culture and Scratch Wound Migration Assay

Human umbilical vein endothelial cells (HUVEC; PromoCell, Heidelberg, Germany) were used between passages 4 and 9 and maintained on 0.1% gelatin-coated plates in Endothelial Growth Medium-2 (EGM-2; Lonza, Basel, Switzerland) at 37 °C and 5% CO_2. For the scratch assay, HUVEC were seeded in 24-well plates (1.2×10^5 cells/well) and grown to confluence. A linear wound was created using a sterile 200 µL pipette tip, detached cells were removed by washing with PBS, and cells were incubated in Endothelial Basal Medium-2 (EBM-2; Lonza) containing 1% DMSO (vehicle control), 250 µM TBZ, an equimolar concentration of MnTBZ, or a 1:1 molar mixture of MnTBZ/MCT-β-CD (TBZ-equivalent concentration).

Images were taken at 0 h and 24 h using a Nikon Eclipse TS100 microscope (Nikon Corporation, Tokyo, Japan) Scratch width was measured in micrometers at three predefined points per well using ImageJ (v. 1.54f, National Institutes of Health, Bethesda, MD, USA), and the mean value was used for calculations. Wound closure (%) was defined as $[1 - (d_{(24h)}/d_{(0h)})] \times 100$, where d_{0h} represents the mean scratch width at 0 h and d_{24h} represents the mean scratch width at 24 h. The experimental design followed the protocol adapted from Cha et al. (2012) [17].

2.4. Statistical Analysis

All experiments were performed in triplicate independent replicates (n = 3), and results are presented as mean ± SD. Statistical significance between treatment groups was assessed

by one-way ANOVA followed by Tukey's post hoc test for multiple comparisons. Differences were considered statistically significant at $p < 0.05$. Data processing and graph generation were carried out using GraphPad Prism 10.6 (GraphPad Software, San Diego, CA, USA).

3. Results

3.1. HUVEC Scratch Assay

In the scratch-wound assay, untreated HUVEC monolayers showed efficient migratory activity and nearly complete wound closure after 24 h (Figure 2).

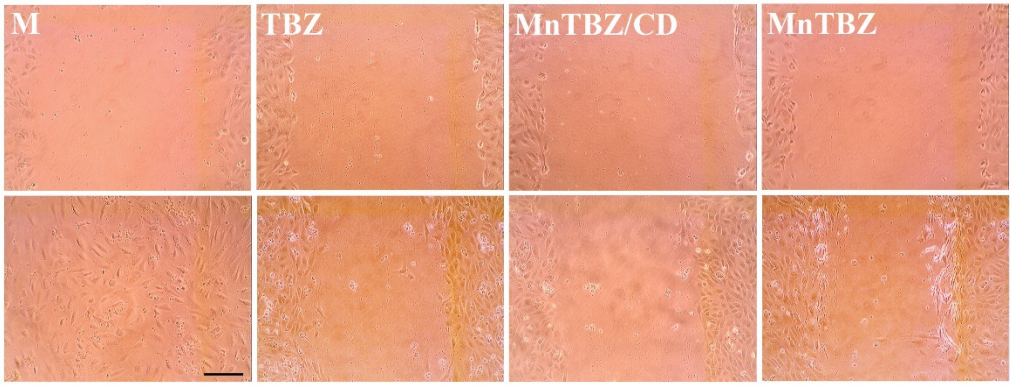

Figure 2. Effect of TBZ, MnTBZ–CD and MnTBZ on HUVEC migration in the scratch-wound assay. Representative phase-contrast images of HUVEC samples immediately after scratching (0 h, **top row**) and after 24 h of treatment (**bottom row**) with the control (M), TBZ, MnTBZ/CD or MnTBZ. Control cells achieved full closure at 24 h, whereas TBZ-based treatments left substantial residual wound gaps (TBZ: ~600 µm; MnTBZ–CD: ~570 µm; MnTBZ: ~500 µm), consistent with the reduced closure percentages observed in the quantitative analysis. TBZ produced the strongest inhibition, followed by MnTBZ–CD and MnTBZ. Scale bar = 200 µm.

Cells exposed to free TBZ showed the strongest inhibition, leaving a residual wound width of 600 ± 30 µm, corresponding to 31.8 ± 5.6% closure and 68% inhibition. The MnTBZ–CD formulation produced a similar but slightly weaker effect, with a remaining gap of 570 ± 30 µm (35.23 ± 5.7% closure, 65% inhibition). MnTBZ alone exhibited the mildest inhibition, with a residual width of 500 ± 30 µm, corresponding to 43.1 ± 5.9% closure and 57% inhibition. These numerical results align with the visual assessment, demonstrating that all three formulations significantly reduced endothelial migration compared with the untreated control, with TBZ exerting the strongest anti-migratory effect and MnTBZ–CD and MnTBZ showing similar but less pronounced inhibition.

At baseline (0 h), the scratch width was consistent across all conditions. After 24 h, the control samples showed almost complete wound closure, whereas all treated groups displayed substantially larger remaining wound distances, indicating reduced endothelial migratory capacity (Figure 3).

One-way ANOVA demonstrated a highly significant overall treatment effect ($p < 0.0001$). Tukey's multiple comparisons test confirmed that all three treatments differed significantly from the control (adjusted $p < 0.0001$ for TBZ, MnTBZ–CD, and MnTBZ). Comparisons among the treatments showed that TBZ inhibited migration significantly more than MnTBZ ($p = 0.0333$), while TBZ vs. MnTBZ–CD and MnTBZ–CD vs. MnTBZ were not statistically significant. These results indicate that although TBZ exerts the strongest inhibitory effect, MnTBZ–CD and MnTBZ reduce wound closure to a similar degree.

At 24 h, the scratch assay revealed marked differences in wound repair among the tested conditions (Figure 3b).

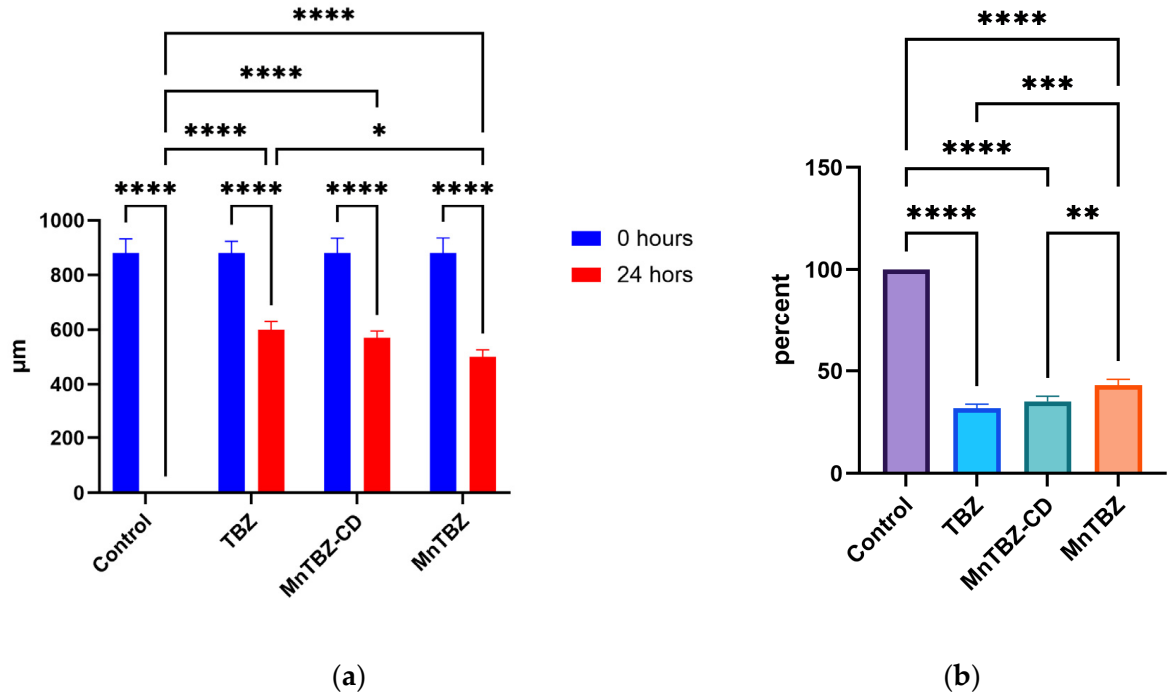

(**a**) (**b**)

Figure 3. Effects of TBZ, MnTBZ–CD, and MnTBZ on HUVEC migration in the scratch-wound assay: (**a**) Scratch-wound distance (µm) measured at 0 h (blue) and 24 h (red) in HUVEC monolayers treated with Control, TBZ, MnTBZ–CD, or MnTBZ. Control cultures achieved near-complete wound closure by 24 h, whereas all treatment groups retained substantial wound gaps, indicating reduced migratory activity. (**b**) Wound closure percentage after 24 h, calculated as (initial scratch width − final scratch width)/initial scratch width × 100. All TBZ-based formulations significantly decreased wound closure relative to Control. Data are presented as mean ± SD (n = 3). Statistical significance was assessed by one-way ANOVA with Tukey's post hoc test. Asterisks indicate significant differences versus Control or between treatment groups (* $p < 0.05$; ** $p < 0.01$; *** $p < 0.001$; **** $p < 0.0001$).

Tukey's multiple comparisons test confirmed that all three treatments showed significantly higher inhibition of wound closure compared with the control (TBZ: 68.20%, MnTBZ–CD: 64.77%, MnTBZ: 56.90%; all adjusted $p < 0.0001$). Comparisons among the treatments further showed that TBZ and MnTBZ–CD did not differ significantly from each other, indicating similar levels of inhibition. However, TBZ exhibited significantly stronger inhibition than MnTBZ ($p = 0.0004$), and MnTBZ–CD also inhibited migration significantly more than MnTBZ ($p = 0.0046$). Overall, the statistical analysis demonstrates a clear gradient of anti-migratory activity, with TBZ and MnTBZ–CD producing the strongest inhibition and MnTBZ showing a comparatively weaker, but still significant, effect.

3.2. pH-Dependent Dissolution Profiles of TBZ, MnTBZ, and MnTBZ–CD

At pH 1.2, all three formulations demonstrated rapid dissolution, with clear differences in early-phase kinetics (Figure 4).

TBZ showed the steepest initial increase, surpassing 70% dissolution by the 5 min time point and exceeding 80% by 10 min. MnTBZ and MnTBZ–CD displayed slower initial profiles, reaching approximately 50–65% at 10 min, but both continued to increase and converged with TBZ between 15 and 20 min. After this initial phase, all formulations reached a stable plateau near 85–90% dissolution, which remained constant throughout the 360 min interval. Two-way ANOVA demonstrated a significant effect of time and formulation (both $p < 0.0001$), confirming that the compounds differ in their early dissolution kinetics, whereas the later plateau phase shows no substantial divergence between the three formulations.

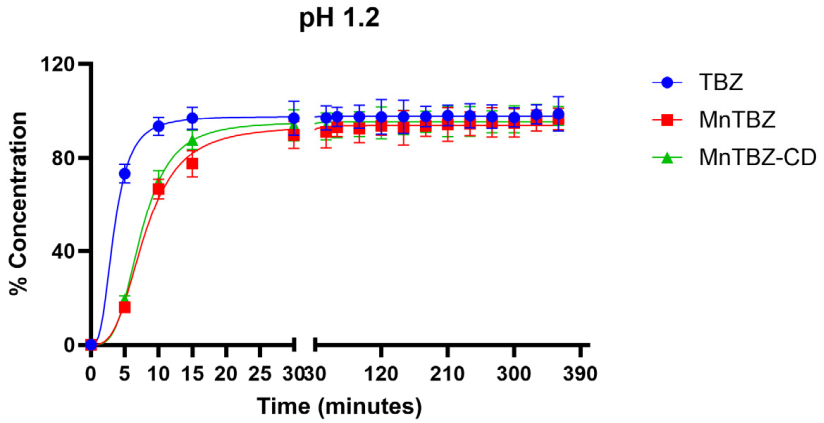

Figure 4. Dissolution profiles of TBZ, MnTBZ, and MnTBZ–CD at pH 1.2. Time-dependent dissolution of TBZ, MnTBZ and the MnTBZ–CD expressed as percentage of dissolved compound over a 360 min interval. Curves represent mean ± SD (n = 3). TBZ showed the fastest initial dissolution, reaching >80% within the first 10 min. MnTBZ and MnTBZ–CD exhibited slower early-phase dissolution but reached comparable plateau values after approximately 20 min. All formulations approached near-complete dissolution by 30 min and maintained stable levels thereafter.

At pH 4.5, clear formulation-dependent differences in dissolution behavior were observed (Figure 5).

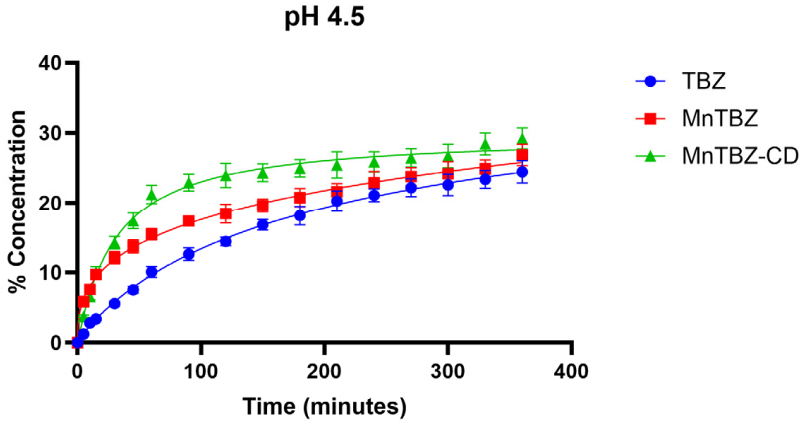

Figure 5. Dissolution profiles of TBZ, MnTBZ, and MnTBZ–CD at pH 4.5. Dissolution kinetics of TBZ, MnTBZ, and MnTBZ–CD in a pH 4.5 medium over a 360 min interval. Data are expressed as mean ± SD (n = 3). MnTBZ–CD displayed the highest dissolution across all time points, followed by MnTBZ and TBZ. All three compounds showed a progressive increase in the dissolved fraction, reaching stable plateau values beginning around 180 min.

MnTBZ–CD exhibited the most pronounced solubility enhancement, achieving approximately 15% dissolution by the 15 min mark and increasing steadily to values above 25% by the end of the experiment. MnTBZ showed intermediate performance, with dissolution rising from ~5% at early time points to around 24% at 360 min. TBZ consistently presented the lowest values, beginning near 2–3% and gradually approaching ~23% at the plateau phase. Two-way ANOVA confirmed significant effects of both formulation and time ($p < 0.0001$ for both factors), as well as a significant interaction ($p < 0.001$), indicating that the dissolution kinetics differed meaningfully among the three compounds across the entire time course.

At pH 6.8, distinct solubility patterns were observed among the three formulations (Figure 6).

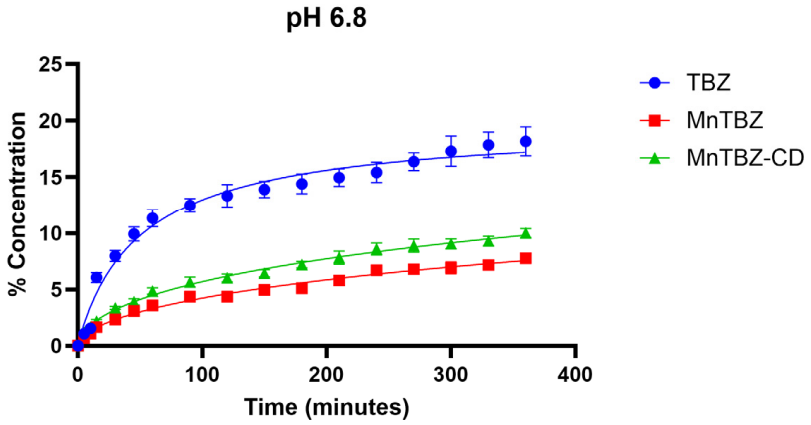

Figure 6. Dissolution profiles of TBZ, MnTBZ, and MnTBZ–CD at pH 6.8. Dissolution kinetics of TBZ, MnTBZ, and MnTBZ–CD in a pH 6.8 medium over a 360 min interval. Values represent mean ± SD (n = 3). TBZ showed the most pronounced increase in dissolved fraction over time, followed by MnTBZ–CD and MnTBZ. All three compounds demonstrated a gradual and sustained rise in solubility throughout the monitored period.

TBZ exhibited the highest dissolution across all time points, rising rapidly during the first 30 min and continuing with a moderate upward trajectory to reach values close to 18% by 360 min. MnTBZ–CD displayed an intermediate profile, increasing steadily and approaching approximately 10% at the final time point. MnTBZ presented the lowest overall dissolution, showing a gradual increase that plateaued near 7–8%. Two-way ANOVA demonstrated statistically significant effects of both formulation and time ($p < 0.0001$ for both), as well as a significant interaction between the two factors ($p < 0.0001$), confirming that the dissolution kinetics differed across the three compounds throughout the observation period.

At pH 7.4, dissolution proceeded more slowly compared with acidic conditions, yet clear formulation-dependent differences were observed (Figure 7).

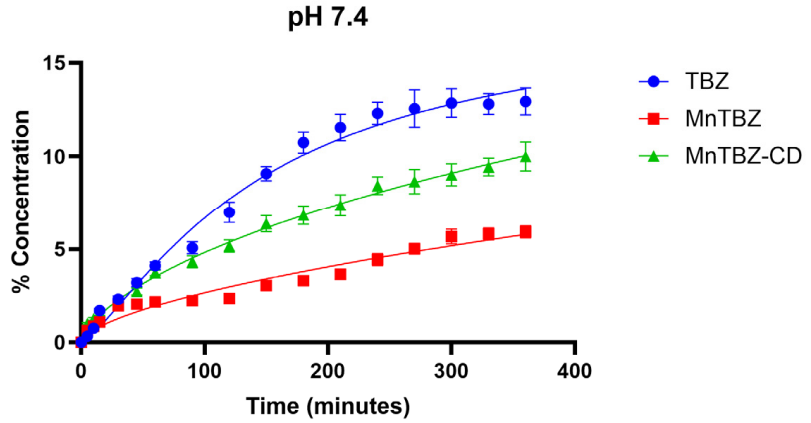

Figure 7. Dissolution profiles of TBZ, MnTBZ, and MnTBZ–CD at pH 7.4. Dissolution curves of TBZ, MnTBZ, and MnTBZ–CD in buffered medium at pH 7.4 over a 360 min interval. Data are shown as mean ± SD (n = 3). TBZ displayed the highest solubility across all measured time points, followed by MnTBZ–CD and MnTBZ. All formulations demonstrated a gradual increase in dissolved fraction throughout the experiment.

TBZ consistently exhibited the highest solubility, increasing steadily from early time points and reaching values above 13% by the end of the experiment. MnTBZ–CD showed an intermediate profile, with dissolution rising progressively to approximately 10% at 360 min. MnTBZ demonstrated the lowest overall solubility, increasing gradually but

remaining below 7% throughout the entire period. Two-way ANOVA indicated significant main effects of formulation and time (both $p < 0.0001$), as well as a significant interaction between formulation and time ($p < 0.0001$), confirming that dissolution kinetics differed substantially among the three compounds at physiological pH.

4. Discussion

TBZ, a benzimidazole derivative originally developed as a broad-spectrum anthelmintic agent, has gained increasing scientific interest in recent years following the discovery of its antiangiogenic properties [17,38]. Beyond its classical antiparasitic mechanism, TBZ has been shown to inhibit the formation of new blood vessels by interfering with microtubule dynamics and with the VEGF-mediated signaling pathways. This ability to modulate endothelial cell behavior and to disrupt key steps of angiogenesis positions it among the potential vascular disrupting agents with antineoplastic relevance [20,39]. In the present study, the antiangiogenic potential of free TBZ and its manganese complex (MnTBZ) was comparatively evaluated using an in vitro scratch assay on HUVEC cells. The obtained results showed that both compounds significantly reduced endothelial cell migration and wound closure capacity compared to the control, with the inhibitory effect being stronger for the free TBZ. To further explore whether these biological differences could be related to physicochemical behavior, dissolution assessments were performed for all tested substances, including the 1:1 cyclodextrin formulation. These analyses confirmed the markedly lower solubility of the MnTBZ complex across the tested pH range, a feature that likely limited its apparent in vitro activity. Nevertheless, such a property might, under physiological conditions, confer a distinct profile, suggestive of a slower dissolution of TBZ.

Across all pH conditions, with the exception of pH 4.5, manganese complexation had the clear effect of slowing the dissolution rate and reducing the extent of TBZ release relative to the free drug. This is attributable to the poor aqueous solubility of the coordination complex itself [40,41]. The complex MnTBZ is a stable, water-insoluble solid, so TBZ must first detach from Mn^{2+} (e.g., via protonation or ligand exchange) to enter solution [42,43]. At low pH (1.2), this detachment can occur readily (protonating TBZ promotes complex dissociation), allowing the complex eventually to release most of its TBZ content, albeit at a slower pace. At pH 4.5, which lies in a mildly acidic range, partial protonation of the TBZ ligand is likely to facilitate limited dissociation or loosening of the MnTBZ structure and/or improve wetting of the solid surface, allowing a slightly larger fraction of ligand to partition into the aqueous phase. In contrast, free TBZ is expected to display reduced solubility near this pH, where it is less extensively ionized, so its dissolved fraction remains lower than that of the complex. At higher pH, however, the complex remains largely intact, reducing TBZ availability. In essence, MnTBZ behaves as a pH-responsive formulation: it is relatively inert in neutral media but can release TBZ in acidic environments [40,44–46].

This pattern suggests a potential for site-specific or sustained release. A MnTBZ complex could, for instance, undergo partial dissociation in the highly acidic gastric environment and then release little additional drug until encountering similarly acidic microenvironments at the tissue or cellular level. A practical limitation, however, is the risk of incomplete dissociation and reduced systemic bioavailability; if the complex remains largely intact, a significant fraction of the dose may simply transit the gastrointestinal tract unabsorbed [47–49]. The incomplete dissolution observed at pH 6.8–7.4 is therefore more compatible with local or targeted administration than with oral systemic delivery [50–53]. In this context, metal complexation clearly modulates the release rate—attenuating the rapid initial dissolution of free TBZ in acid—but at the cost of introducing a solubility constraint that would need to be addressed for broader therapeutic use. These findings

are in line with general pharmaceutical experience that reducing drug solubility tends to prolong release, but attention should be given to the fact that when solubility becomes excessively low the formulation may release the drug too slowly to achieve adequate bioavailability [54–56]. Notably, complexation of benzimidazoles with metals has been explored in other contexts, often to alter biological activity or targeting without considering the solubility [57,58]. Formulation strategies to address this could include using the complex in a capsule with acidic excipients (to promote its dissolution in vivo) or co-administering with solubilizing agents [50,59,60].

Inclusion of MCT-β-CD in the formulation had a beneficial impact on TBZ dissolution, consistent with the extensive literature on CD–azole interactions [61–63]. CD are well-known to increase the aqueous solubility and dissolution rate of poorly water-soluble drugs by forming inclusion complexes [28,64]. In the present study, mixing MCT-β-CD with the MnTBZ complex improved TBZ solubility at all pH levels tested (though to varying degrees). The probable mechanism is that MCT-β-CD molecules can host the lipophilic TBZ inside their hydrophobic cavity, thereby keeping in solution a surplus of TBZ molecules which would otherwise precipitate. At pH 1.2, as discussed, the effect of MCT-β-CD was minimal because MnTBZ was already soluble as the protonated form. However, at pH 4.5 the MCT-β-CD mixture achieved a slightly higher dissolved fraction than MnTBZ alone, and at pH 6.8–7.4 MCT-β-CD almost doubled the amount of dissolved TBZ (from ~5% to ~10% at neutral pH in 5 h, as noted above). While this is still lower than free TBZ, it demonstrates the principle that MCT-β-CD can prevent TBZ from crystallizing out. Every TBZ molecule that dissociates can be immediately encapsulated by CD, which would maintain the concentration gradient for further dissolution [65,66].

Our findings align with prior studies on TBZ and related benzimidazoles. For example, Gao et al. (2020) reported that forming an inclusion complex of TBZ with hydroxypropyl-β-CD increased the fungicidal efficacy of TBZ by improving its water solubility [67]. In their work, an electrospun TBZ/hydroxypropyl-β-CD nanofiber showed fast disintegration and enhanced antifungal activity compared to TBZ alone, thanks to rapid drug release. Likewise, for the antiparasitic albendazole (another BCS Class II benzimidazole), methyl-β-cyclodextrin complexation raised solubility by an astounding ~150,000-fold and enabled >90% of the drug to dissolve in 10 min [31]. These examples underscore how effective cyclodextrin inclusion can be in overcoming dissolution limitations. Our approach demonstrated improved dissolution, reinforcing the relevance of CD as solubilizing excipients for TBZ. In a future study a comparison could indicate if a pre-formed TBZ-CD inclusion complex or a ternary complex with Mn^{2+} would further boost dissolution.

It is worth noting that pH can influence CD efficacy. TBZ has maximal solubility around pH 2.5, and its neutral form predominates at pH > 5 [40,42]. While CD can include neutral TBZ, the stability of the complex and the overall solubilization may differ across pH [65,68]. In practice, however, the inclusion strategy appears broadly beneficial whenever TBZ is in a poorly soluble state (e.g., in the intestine). Thus, combining TBZ (or MnTBZ complexes) with CD emerges as a promising strategy to ensure adequate release in the target absorption window [69].

Although TBZ was originally introduced as a broad-spectrum anthelmintic, its antiparasitic mechanism of action shares distinct structural and functional parallels with that underlying its antiangiogenic effects. In both cases, the primary molecular target is the microtubule network, a fundamental component of the cellular cytoskeleton [17,70]. In parasitic organisms, TBZ binds to β-tubulin and inhibits microtubule polymerization, disrupting glucose transport and mitotic progression, ultimately leading to parasite death [71,72]. Similarly, in human endothelial cells, TBZ interferes with microtubule organization, causing cytoskeletal destabilization that compromises cell migration, alignment, and capillary-like

structure formation [20]. This perturbation of microtubule dynamics also affects VEGF-dependent signaling cascades—particularly the Rho/ROCK and FAK pathways—resulting in marked inhibition of angiogenesis [17].

In the present study, after 24 h, the control HUVEC samples achieved complete wound closure, reflecting preserved migratory capacity. In contrast, all TBZ-based treatments markedly impaired endothelial movement. Cells exposed to free TBZ showed the strongest inhibition, leaving a residual wound width of 600 ± 30 µm, corresponding to 31.8 ± 5.6% closure. The MnTBZ–CD formulation showed a slightly weaker effect, with a remaining gap of 570 ± 30 µm and a wound closure of 35.23 ± 5.7%. MnTBZ exhibited the mildest inhibition among the three treatments, with a residual width of 500 ± 30 µm and 43.1 ± 5.9% closure. These results demonstrate that all three formulations significantly reduced endothelial migration relative to the control, with free TBZ exerting the strongest anti-migratory effect. The lower activity of the manganese complex may be related to its limited solubility or bioavailability in the culture medium, whereas cyclodextrin complexation appears to partially enhance dispersion and improve its inhibitory profile.

Similar trends have been reported for other benzimidazole derivatives, where metal complexation modulated pharmacodynamic activity primarily through changes in solubility and molecular accessibility rather than intrinsic loss of function [58,73]. In particular, it was demonstrated that albendazole inhibits endothelial cell proliferation, migration, and tube formation in HUVECs through microtubule destabilization and downregulation of VEGF signaling [74]. Furthermore, studies on metal–benzimidazole complexes have shown that coordination to transition metals such as Cu(II), Ni(II), or Mn(II) often alters the physicochemical profile—particularly aqueous solubility and permeability—thereby modulating biological efficacy in both antimicrobial and cytotoxic assays [57].

Taken together, our data reinforce the view that TBZ is a repurposable agent that combines well-established anthelmintic and antifungal activity with preclinically demonstrated antiangiogenic effects [17]. From an infectious-disease perspective, this dual profile is conceptually attractive, as angiogenesis and vascular remodeling are increasingly recognized as important components of the tissue response to chronic infection. In mycobacterial disease, for example, granulomas become vascularized through VEGF-dependent pathways, and abnormal granuloma vasculature has been implicated in supporting bacterial growth and limiting efficient drug delivery [75,76]. Leishmania infections and invasive fungal diseases likewise induce marked vascular and lymphatic remodeling in affected tissues, which shapes local inflammation and pathogen–host interactions [77,78]. Although TBZ's antiangiogenic activity has so far been investigated mainly in cancer and developmental models, it is tempting to speculate that benzimidazole-based vascular disrupting agents could, in principle, be explored as host-directed adjuvants in selected infectious settings, where modulating pathological neovascularization might complement direct antimicrobial therapy. Future work would benefit from incorporating in vivo infection models to determine whether modulating angiogenesis with TBZ or its derivatives influences tissue vascularity, immune microenvironments, or pathogen control, thereby clarifying the potential relevance of these mechanisms beyond the in vitro setting.

The pharmacological and formulation-related findings obtained in this study have broader implications for the potential repositioning of TBZ as a multifunctional therapeutic scaffold. The observed reduction in endothelial migration induced by free TBZ underscores its direct antiangiogenic capacity, yet the altered behavior of its manganese complex highlights the delicate balance between molecular modification and pharmacological performance.

The marked insolubility of MnTBZ across physiological pH values, while limiting in vitro activity, may under certain circumstances provide a controlled or site-dependent

release pattern. Such a property could be advantageous in localized therapeutic contexts—such as gastrointestinal antiparasitic therapy—where sustained luminal exposure rather than systemic absorption is desired. Conversely, for systemic antiangiogenic or antifungal applications, the slow and incomplete dissociation of the complex may limit overall bioavailability, suggesting that further formulation refinement could help balance complex stability with efficient drug release.

The inclusion of MCT-β-CD in the formulation represents one such optimization strategy. By improving aqueous dispersion and maintaining TBZ in a soluble form upon dissociation from the complex, CD not only enhances dissolution kinetics but may also reduce interindividual variability in absorption. This approach aligns with extensive pharmaceutical evidence showing that supramolecular inclusion can transform poorly soluble benzimidazoles into bioavailable and therapeutically effective entities. Further refinement, such as pre-forming ternary complexes involving TBZ, Mn^{2+}, and CD, or embedding these systems within nanoparticulate or polymeric matrices, could enable tunable release profiles suitable for either systemic or localized therapeutic goals.

As this work represents an initial, proof-of-concept evaluation, several aspects remain to be explored in future studies. Our findings are based on in vitro dissolution testing and a single endothelial migration model, which, while appropriate for preliminary assessment, cannot fully capture the complexity of in vivo angiogenic or infectious environments. In addition, although the MnTBZ complex and the cyclodextrin mixture were prepared following previously validated procedures, more detailed physicochemical characterization and exploration of alternative formulation strategies may further clarify their performance.

5. Conclusions

The present study highlights the versatile nature of TBZ as both an antiparasitic and antiangiogenic compound, with biological performance that can be modulated through metal–ligand chemistry and formulation design. The comparison between free TBZ, its manganese complex, and the CD-containing formulation demonstrates how even small-scale molecular and supramolecular adjustments can markedly influence solubility, release kinetics, and ultimately biological efficacy. These observations not only extend the pharmacological relevance of TBZ beyond its classical use but also exemplify the broader concept of repurposing established antiparasitic chemical frameworks as host-targeted modulators of angiogenesis and infection. Further studies integrating in vitro and in vivo approaches will be essential to define the translational potential of these systems and to harness their dual activity for therapeutic innovation in both infectious and angiogenesis-dependent diseases.

Author Contributions: Conceptualization, C.-E.L., L.O., A.D.C. and B.A.S.; methodology, C.-E.L., L.O., L.S., L.G.F., B.M., V.C. and O.O.; validation, L.O., L.G.F., C.I.F., V.C., O.O., A.D.C. and B.A.S.; formal analysis, B.M., C.I.F., O.O. and B.A.S.; investigation, C.-E.L., L.S., L.G.F., C.I.F., V.C., A.D.C. and B.A.S.; resources, C.-E.L., L.O., L.G.F. and B.A.S.; data curation, C.-E.L., L.S., B.M., O.O., A.D.C. and B.A.S.; writing—original draft preparation, C.-E.L., L.O., L.S., L.G.F., C.I.F., A.D.C. and B.A.S.; writing—review and editing, C.-E.L., L.O., L.S., L.G.F., B.M., V.C., O.O., A.D.C. and B.A.S.; visualization, B.M. and B.A.S.; supervision, C.-E.L., L.O. and B.A.S.; project administration, C.-E.L., L.O., V.C., A.D.C. and B.A.S. All authors have read and agreed to the published version of the manuscript.

Funding: This research received no external funding.

Institutional Review Board Statement: HUVEC cells were purchased from PromoCell (Heidelberg, Germany). Cells were obtained from an approved donor program, and all ethical approvals for tissue collection were handled by the supplier. No additional local ethical approval was required for this study.

Data Availability Statement: The datasets generated and analyzed in this study form part of a larger ongoing research project and are therefore not publicly available at this time. The data may be made available in the future, following completion and publication of the full study, upon reasonable request to the corresponding author.

Acknowledgments: The authors declare that no generative artificial intelligence (GenAI) tools were used in the preparation of this manuscript, including in the writing, data analysis, study design, figure creation, or interpretation of results. All content was produced, reviewed, and edited exclusively by the authors.

Conflicts of Interest: The authors declare no conflicts of interest.

Abbreviations

The following abbreviations are used in this manuscript:

TBZ	Thiabendazole
MnTBZ	Manganese–thiabendazole complex
CD	Cyclodextrin
MCT-β-CD	Monochlorotriazynyl-β-cyclodextrin
DMSO	Dimethyl sulfoxide
USP	United States Pharmacopeia
UV–VIS	Ultraviolet–visible spectroscopy
SD	Standard deviation
HUVECs	Human umbilical vein endothelial cells
EGM-2	Endothelial Growth Medium-2
EBM-2	Endothelial Basal Medium-2
PBS	Phosphate-buffered saline
VEGF	Vascular endothelial growth factor
FAK	Focal adhesion kinase
ROCK	Rho-associated protein kinase
MRI	Magnetic resonance imaging
MOF	Metal–organic framework
DFT	Density functional theory
M	Medium (control condition in figures)
n	Number of replicates

References

1. Carmeliet, P. Angiogenesis in Life, Disease and Medicine. *Nature* **2005**, *438*, 932–936. [CrossRef] [PubMed]
2. Herbert, S.P.; Stainier, D.Y.R. Molecular Control of Endothelial Cell Behaviour during Blood Vessel Morphogenesis. *Nat. Rev. Mol. Cell Biol.* **2011**, *12*, 551–564. [CrossRef]
3. Folkman, J. Angiogenesis: An Organizing Principle for Drug Discovery? *Nat. Rev. Drug Discov.* **2007**, *6*, 273–286. [CrossRef]
4. Kerbel, R.S. Tumor Angiogenesis. *N. Engl. J. Med.* **2008**, *358*, 2039–2049. [CrossRef]
5. Liu, Z.-L.; Chen, H.-H.; Zheng, L.-L.; Sun, L.-P.; Shi, L. Angiogenic Signaling Pathways and Anti-Angiogenic Therapy for Cancer. *Signal Transduct. Target. Ther.* **2023**, *8*, 198. [CrossRef] [PubMed]
6. Wang, L.; Liu, W.-Q.; Broussy, S.; Han, B.; Fang, H. Recent Advances of Anti-Angiogenic Inhibitors Targeting VEGF/VEGFR Axis. *Front. Pharmacol.* **2024**, *14*, 1307860. [CrossRef] [PubMed]
7. Gacche, R.N. Changing Landscape of Anti-Angiogenic Therapy: Novel Approaches and Clinical Perspectives. *Biochim. Biophys. Acta (BBA) Rev. Cancer* **2023**, *1878*, 189020. [CrossRef]
8. Guo, B.; Li, Z.; Zhou, J.; Shu, R.; Wei, W.; Kuang, Y.; Xu, Y.; Wu, X. Anti-Neoangiogenic Nanodelivery Systems: Advances in Tumor-Based and Ophthalmic Disease Research. *J. Mater. Chem. B* **2025**, *13*, 13527–13566. [CrossRef]
9. Vasudev, N.S.; Reynolds, A.R. Anti-Angiogenic Therapy for Cancer: Current Progress, Unresolved Questions and Future Directions. *Angiogenesis* **2014**, *17*, 471–494. [CrossRef]
10. Stone, R.L.; Sood, A.K.; Coleman, R.L. Collateral Damage: Toxic Effects of Targeted Antiangiogenic Therapies in Ovarian Cancer. *Lancet Oncol.* **2010**, *11*, 465–475. [CrossRef]

11. Sherafat, N.S.; Keshavarz, A.; Mardi, A.; Mohammadiara, A.; Aghaei, M.; Aghebati-Maleki, L.; Mohammadi, M.H. Rationale of Using Immune Checkpoint Inhibitors (ICIs) and Anti-Angiogenic Agents in Cancer Treatment from a Molecular Perspective. *Clin. Exp. Med.* **2025**, *25*, 238. [CrossRef]
12. Athul, H.; Shaji, S.; Shabik, K.; Joseph, A. Harnessing the Power of Drug Repurposing: A Promising Strategy for Drug Discovery and Development. *Natl. J. Pharmacol. Ther.* **2024**, *2*, 123. [CrossRef]
13. Bhatia, T.; Sharma, S. Drug Repurposing: Insights into Current Advances and Future Applications. *Curr. Med. Chem.* **2025**, *32*, 468–510. [CrossRef]
14. Xia, Y.; Sun, M.; Huang, H.; Jin, W.-L. Drug Repurposing for Cancer Therapy. *Signal Transduct. Target. Ther.* **2024**, *9*, 92. [CrossRef] [PubMed]
15. Recino, A.; Rayner, M.L.D.; Rohn, J.L.; Della Pasqua, O.; Recino, A.; Rayner, M.L.D.; Rohn, J.L.; Carter, B.; Cupani, A.; Dahlmann-Noor, A.; et al. Therapeutic Innovation in Drug Repurposing: Challenges and Opportunities. *Drug Discov. Today* **2025**, *30*, 104390. [CrossRef] [PubMed]
16. Zhang, C.; Zhong, B.; Yang, S.; Pan, L.; Yu, S.; Li, Z.; Li, S.; Su, B.; Meng, X. Synthesis and Biological Evaluation of Thiabendazole Derivatives as Anti-Angiogenesis and Vascular Disrupting Agents. *Bioorg Med. Chem.* **2015**, *23*, 3774–3780. [CrossRef]
17. Cha, H.J.; Byrom, M.; Mead, P.E.; Ellington, A.D.; Wallingford, J.B.; Marcotte, E.M. Evolutionarily Repurposed Networks Reveal the Well-Known Antifungal Drug Thiabendazole to Be a Novel Vascular Disrupting Agent. *PLoS Biol.* **2012**, *10*, e1001379. [CrossRef]
18. Zalewski, J.; Szajna, M.; Stępień, K.; Nowak, K.; Karcińska, A.; Yika, A.d.C.; Krawczyk, K.; Karwat, K.; Zalewska, M.; Pierzchalski, P. Endothelial Cell Apoptosis but Not Necrosis Is Inhibited by Ischemic Preconditioning. *Int. J. Mol. Sci.* **2024**, *25*, 1238. [CrossRef] [PubMed]
19. Qi, W.; Xu, G.; Tang, L.; Ye, C.; Liu, X. Exploring the Therapeutic Role of Thiabendazole in Lung Adenocarcinoma via Network Pharmacology and Single-Cell Analysis. *Transl. Oncol.* **2025**, *62*, 102548. [CrossRef]
20. Garge, R.K.; Cha, H.J.; Lee, C.; Gollihar, J.D.; Kachroo, A.H.; Wallingford, J.B.; Marcotte, E.M. Discovery of New Vascular Disrupting Agents Based on Evolutionarily Conserved Drug Action, Pesticide Resistance Mutations, and Humanized Yeast. *Genetics* **2021**, *219*, iyab101. [CrossRef]
21. Morbidelli, L.; Donnini, S.; Filippi, S.; Messori, L.; Piccioli, F.; Orioli, P.; Sava, G.; Ziche, M. Antiangiogenic Properties of Selected Ruthenium(III) Complexes That Are Nitric Oxide Scavengers. *Br. J. Cancer* **2003**, *88*, 1484–1491. [CrossRef]
22. Hamali, M.A.; Roney, M.; Dubey, A.; Uddin, M.N.; Zulkifli, N.A.; Fasihi Mohd Aluwi, M.F.; Musa, M.; Tajuddin, A.M.; Kassim, K. Cu(II) Complexes Based on Benzimidazole Ligands: Synthesis, Characterization, DFT, Molecular Docking & Bioactivity Study. *Future Med. Chem.* **2024**, *16*, 2535–2546. [CrossRef]
23. Saha, A.; Debnath, A.; Chettri, M.; Mahato, R.K.; Das, D.; Sarkar, D.; Chaurasia, R.; Bhattacharyya, S.; Mukherjee, M.; Biswas, B. Benzimidazole-Coordinated Copper(II) Complexes as Effectual Chemotherapeutics against Malignancy. *ACS Omega* **2025**, *10*, 34399–34413. [CrossRef] [PubMed]
24. Zheng, R.; Guo, J.; Cai, X.; Bin, L.; Lu, C.; Singh, A.; Trivedi, M.; Kumar, A.; Liu, J. Manganese Complexes and Manganese-Based Metal-Organic Frameworks as Contrast Agents in MRI and Chemotherapeutics Agents: Applications and Prospects. *Colloids Surf. B Biointerfaces* **2022**, *213*, 112432. [CrossRef]
25. Kim, W.K.; An, J.M.; Lim, Y.J.; Kim, K.; Kim, Y.H.; Kim, D. Recent Advances in Metallodrug: Coordination-Induced Synergy between Clinically Approved Drugs and Metal Ions. *Mater. Today Adv.* **2025**, *25*, 100569. [CrossRef]
26. Samineni, R.; Chimakurthy, J.; Konidala, S. Emerging Role of Biopharmaceutical Classification and Biopharmaceutical Drug Disposition System in Dosage Form Development: A Systematic Review. *Turk. J. Pharm. Sci.* **2022**, *19*, 706–713. [CrossRef] [PubMed]
27. Saokham, P.; Muankaew, C.; Jansook, P.; Loftsson, T. Solubility of Cyclodextrins and Drug/Cyclodextrin Complexes. *Molecules* **2018**, *23*, 1161. [CrossRef]
28. Spiridon, I.; Anghel, N. Cyclodextrins as Multifunctional Platforms in Drug Delivery and Beyond: Structural Features, Functional Applications, and Future Trends. *Molecules* **2025**, *30*, 3044. [CrossRef] [PubMed]
29. Pyrak, B.; Gubica, T.; Rogacka-Pyrak, K. Cyclodextrin Nanosponges as Bioenhancers of Phytochemicals. *Prospect. Pharm. Sci.* **2024**, *22*, 170–177. [CrossRef]
30. Napiórkowska, E. Overview of cyclodextrins and medicinal products containing cyclodextrins currently registered in Poland. *Prospect. Pharm. Sci.* **2023**, *21*, 30–37. [CrossRef]
31. Ding, Y.; Zhang, Z.; Ding, C.; Xu, S.; Xu, Z. The Use of Cyclodextrin Inclusion Complexes to Increase the Solubility and Pharmacokinetic Profile of Albendazole. *Molecules* **2023**, *28*, 7295. [CrossRef]
32. Yan, H.; Zhong, X.; Liu, Y. Improving the Solubility, Stability, and Bioavailability of Albendazole through Synthetic Salts. *Molecules* **2024**, *29*, 3571. [CrossRef]
33. Khobragade, P.P.; Manvatkar, V.; Meshram, P.; Dongre, R. Multi-Purpose Cyclodextrin Metal-Complexes: Physicochemical and Theoretical Portfolio in Drug Domain. *J. Chem. Health Risks* **2024**, *14*, 1121–1136.

34. Rizzarelli, E.; Vecchio, G. Metal Complexes of Functionalized Cyclodextrins as Enzyme Models and Chiral Receptors. *Coord. Chem. Rev.* **1999**, *188*, 343–364. [CrossRef]
35. Prochowicz, D.; Kornowicz, A.; Lewiński, J. Interactions of Native Cyclodextrins with Metal Ions and Inorganic Nanoparticles: Fertile Landscape for Chemistry and Materials Science. *Chem. Rev.* **2017**, *117*, 13461–13501. [CrossRef] [PubMed]
36. Kelly, R. *Synthesis, Characterisation and Biological Activity of Transition Metal Complexes of Thiabendazole*; Technological University Dublin: Dublin, Ireland, 2004. [CrossRef]
37. Rajzman, A. Determination of Thiabendazole in Citrus Fruits by Ultraviolet Spectrophotometry. *Analyst* **1974**, *99*, 120–127. [CrossRef] [PubMed]
38. Chai, J.-Y.; Jung, B.-K.; Hong, S.-J. Albendazole and Mebendazole as Anti-Parasitic and Anti-Cancer Agents: An Update. *Korean J. Parasitol.* **2021**, *59*, 189–225. [CrossRef]
39. Elmaaty, A.A.; Darwish, K.M.; Chrouda, A.; Boseila, A.A.; Tantawy, M.A.; Elhady, S.S.; Shaik, A.B.; Mustafa, M.; Al-karmalawy, A.A. In Silico and In Vitro Studies for Benzimidazole Anthelmintics Repurposing as VEGFR-2 Antagonists: Novel Mebendazole-Loaded Mixed Micelles with Enhanced Dissolution and Anticancer Activity. *ACS Omega* **2022**, *7*, 875–899. [CrossRef] [PubMed]
40. El-Nahhal, Y.Z. Development of Controlled Release Formulations of Thiabendazole. *J. Agric. Chem. Environ.* **2014**, *3*, 1–8. [CrossRef]
41. Nielsen, L.S.; Bundgaard, H.; Falch, E. Prodrugs of Thiabendazole with Increased Water-Solubility. *Acta Pharm. Nord.* **1992**, *4*, 43–49.
42. Budetić, M.; Kopf, D.; Dandić, A.; Samardžić, M. Review of Characteristics and Analytical Methods for Determination of Thiabendazole. *Molecules* **2023**, *28*, 3926. [CrossRef]
43. Aeindartehran, L.; Lefton, J.B.; Burleson, J.; Unruh, D.K.; Runčevski, T. Soluble Thiabendazolium Salts with Anthelminthic Properties. *Int. J. Pharm.* **2023**, *647*, 123516. [CrossRef] [PubMed]
44. Roque, J.P.L.; Rosado, M.T.S.; Fausto, R.; Reva, I. Dual Photochemistry of Benzimidazole. *J. Org. Chem.* **2023**, *88*, 2884–2897. [CrossRef]
45. Nixon, J.R.; Hassan, M.A.M. The Effect of pH on the Release Characteristics of Thiabendazole Microcapsules. *Drug Dev. Ind. Pharm.* **1981**, *7*, 305–316. [CrossRef]
46. Kaplan, S.B.; Konçe, İ.; Demiralay, E.Ç. Determination of Protonation Constant Value of Thiabendazole in Ethanol-Water Binary Mixtures by Green RPLC Method. *J. Res. Pharm.* **2025**, *28*, 40–50.
47. Akula, P.; P.K., L. Effect of pH on Weakly Acidic and Basic Model Drugs and Determination of Their *Ex. Vivo* Transdermal Permeation Routes. *Braz. J. Pharm. Sci.* **2018**, *54*, e00070. [CrossRef]
48. Stillhart, C.; Vučićević, K.; Augustijns, P.; Basit, A.W.; Batchelor, H.; Flanagan, T.R.; Gesquiere, I.; Greupink, R.; Keszthelyi, D.; Koskinen, M.; et al. Impact of Gastrointestinal Physiology on Drug Absorption in Special Populations—An UNGAP Review. *Eur. J. Pharm. Sci.* **2020**, *147*, 105280. [CrossRef]
49. Munnangi, S.R.; Youssef, A.A.A.; Narala, N.; Lakkala, P.; Narala, S.; Vemula, S.K.; Repka, M. Drug Complexes: Perspective from Academic Research and Pharmaceutical Market. *Pharm. Res.* **2023**, *40*, 1519–1540. [CrossRef] [PubMed]
50. Su, D.; Bai, M.; Wei, C.; Long, X.; Liu, X.; Shen, X.; Ding, H. Combining Solubilization and Controlled Release Strategies to Prepare pH-Sensitive Solid Dispersion Loaded with Albendazole: In Vitro and in Vivo Studies. *Front. Vet. Sci.* **2024**, *11*, 1522856. [CrossRef]
51. Biswas, M.; Kanta Choudhury, K.; Banerjee, A.; Pathak, R.K. Elevating the Discourse on Drug Delivery: A Fresh Perspective on the Utilization of Coordination Chemistry-Driven Metal-Drug Conjugates. *Coord. Chem. Rev.* **2024**, *517*, 216026. [CrossRef]
52. La Manna, S.; Roviello, V.; Napolitano, F.; Malfitano, A.M.; Monaco, V.; Merlino, A.; Monti, M.; Kowalski, K.; Szczupak, Ł.; Marasco, D. Metal-Complexes Bearing Releasable CO Differently Modulate Amyloid Aggregation. *Inorg. Chem.* **2023**, *62*, 10470–10480. [CrossRef] [PubMed]
53. Wong, K.-Y.; Nie, Z.; Wong, M.-S.; Wang, Y.; Liu, J. Metal–Drug Coordination Nanoparticles and Hydrogels for Enhanced Delivery. *Adv. Mater.* **2024**, *36*, 2404053. [CrossRef] [PubMed]
54. Bhalani, D.V.; Nutan, B.; Kumar, A.; Singh Chandel, A.K. Bioavailability Enhancement Techniques for Poorly Aqueous Soluble Drugs and Therapeutics. *Biomedicines* **2022**, *10*, 2055. [CrossRef]
55. Zhang, X.; Xing, H.; Zhao, Y.; Ma, Z. Pharmaceutical Dispersion Techniques for Dissolution and Bioavailability Enhancement of Poorly Water-Soluble Drugs. *Pharmaceutics* **2018**, *10*, 74. [CrossRef] [PubMed]
56. Zhuo, Y.; Zhao, Y.-G.; Zhang, Y. Enhancing Drug Solubility, Bioavailability, and Targeted Therapeutic Applications through Magnetic Nanoparticles. *Molecules* **2024**, *29*, 4854. [CrossRef]
57. Mañozca-Dosman, I.V.; Aragón-Muriel, A.; Polo-Cerón, D. Antibacterial Activity of Metal Complexes of Cu(II) and Ni(II) with the Ligand 2-(Phenylsubstituted) Benzimidazole. *Sci. Pharm.* **2025**, *93*, 22. [CrossRef]
58. Nouman; Rana, M.; Ahmedi, S.; Mehandi, R.; Dhama, M.; Manzoor, N. Rahisuddin Transition Metal Complexes of Benzimidazole-Based Ligands: Synthesis, Characterization, Biological, and Catecholase Activities. *Inorganica Chim. Acta* **2025**, *574*, 122392. [CrossRef]

59. Gupta, S.; Kesarla, R.; Omri, A. Formulation Strategies to Improve the Bioavailability of Poorly Absorbed Drugs with Special Emphasis on Self-Emulsifying Systems. *ISRN Pharm.* **2013**, *2013*, 848043. [CrossRef]
60. Quodbach, J.; Preis, E.; Karkossa, F.; Winck, J.; Finke, J.H.; Steiner, D. Novel Strategies for the Formulation of Poorly Water-Soluble Drug Substances by Different Physical Modification Strategies with a Focus on Peroral Applications. *Pharmaceuticals* **2025**, *18*, 1089. [CrossRef]
61. Shikha, R.; Kar, S.S. Evaluation of Molecular Inclusion of Azole Antifungals by β-Cyclodextrin Using Computational Molecular Approach. *Discov. Chem.* **2024**, *1*, 51. [CrossRef]
62. Hostetler, J.S.; Hanson, L.H.; Stevens, D.A. Effect of Cyclodextrin on the Pharmacology of Antifungal Oral Azoles. *Antimicrob. Agents Chemother.* **1992**, *36*, 477–480. [CrossRef]
63. Leclercq, L.; Nardello-Rataj, V. Pickering Emulsions Based on Cyclodextrins: A Smart Solution for Antifungal Azole Derivatives Topical Delivery. *Eur. J. Pharm. Sci.* **2016**, *82*, 126–137. [CrossRef]
64. Mohammad, A.; Singh, S.; Swain, S. Cyclodextrins: Concept to Applications, Regulatory Issues and Challenges. *Nanomed. Res. J.* **2020**, *5*, 202–214. [CrossRef]
65. Samuelsen, L.; Holm, R.; Lathuile, A.; Schönbeck, C. Correlation between the Stability Constant and pH for β-Cyclodextrin Complexes. *Int. J. Pharm.* **2019**, *568*, 118523. [CrossRef]
66. Swiech, O.; Majdecki, M.; Opuchlik, L.J.; Bilewicz, R. Impact of pH and Cell Medium on the Interaction of Doxorubicin with Lipoic Acid Cyclodextrin Conjugate as the Drug Carrier. *J. Incl. Phenom. Macrocycl. Chem.* **2020**, *97*, 129–136. [CrossRef]
67. Gao, S.; Liu, Y.; Jiang, J.; Li, X.; Zhao, L.; Fu, Y.; Ye, F. Encapsulation of Thiabendazole in Hydroxypropyl-β-Cyclodextrin Nanofibers via Polymer-Free Electrospinning and Its Characterization. *Pest. Manag. Sci.* **2020**, *76*, 3264–3272. [CrossRef]
68. Jambhekar, S.S.; Breen, P. Cyclodextrins in Pharmaceutical Formulations II: Solubilization, Binding Constant, and Complexation Efficiency. *Drug Discov. Today* **2016**, *21*, 363–368. [CrossRef] [PubMed]
69. Crini, G.; Morcellet, M. Synthesis and Applications of Adsorbents Containing Cyclodextrins. *J. Sep. Sci.* **2002**, *25*, 789–813. [CrossRef]
70. Park, S.J.; Song, I.; Yeom, G.S.; Nimse, S.B. The Microtubule Cytoskeleton: A Validated Target for the Development of 2-Aryl-1*H*-Benzo[*d*]Imidazole Derivatives as Potential Anticancer Agents. *Biomed. Pharmacother.* **2024**, *171*, 116106. [CrossRef]
71. Minagawa, M.; Shirato, M.; Toya, M.; Sato, M. Dual Impact of a Benzimidazole Resistant β-Tubulin on Microtubule Behavior in Fission Yeast. *Cells* **2021**, *10*, 1042. [CrossRef]
72. Jasmer, D.P.; Yao, C.; Rehman, A.; Johnson, S. Multiple Lethal Effects Induced by a Benzimidazole Anthelmintic in the Anterior Intestine of the Nematode *Haemonchus contortus*. *Mol. Biochem. Parasitol.* **2000**, *105*, 81–90. [CrossRef] [PubMed]
73. Hussain, A.; AlAjmi, M.F.; Rehman, M.T.; Khan, A.A.; Shaikh, P.A.; Khan, R.A. Evaluation of Transition Metal Complexes of Benzimidazole-Derived Scaffold as Promising Anticancer Chemotherapeutics. *Molecules* **2018**, *23*, 1232. [CrossRef] [PubMed]
74. Pourgholami, M.H.; Khachigian, L.M.; Fahmy, R.G.; Badar, S.; Wang, L.; Chu, S.W.L.; Morris, D.L. Albendazole Inhibits Endothelial Cell Migration, Tube Formation, Vasopermeability, VEGF Receptor-2 Expression and Suppresses Retinal Neovascularization in ROP Model of Angiogenesis. *Biochem. Biophys. Res. Commun.* **2010**, *397*, 729–734. [CrossRef]
75. Oehlers, S.H.; Cronan, M.R.; Beerman, R.W.; Johnson, M.G.; Huang, J.; Kontos, C.D.; Stout, J.E.; Tobin, D.M. Infection-Induced Vascular Permeability Aids Mycobacterial Growth. *J. Infect. Dis.* **2017**, *215*, 813–817. [CrossRef]
76. Osherov, N.; Ben-Ami, R. Modulation of Host Angiogenesis as a Microbial Survival Strategy and Therapeutic Target. *PLoS Pathog.* **2016**, *12*, e1005479. [CrossRef]
77. Fry, L.; de Jesus, F.N.; Carneiro, M.B.; Roys, H.; Bowlin, A.; Peters, N.C.; von der Weid, P.-Y.; Weinkopff, T. Dysregulated Lymphatic Remodeling Promotes Immunopathology during Non-Healing Cutaneous Leishmaniasis. *bioRxiv* **2025**. bioRxiv:2025.05.01.651666. [CrossRef]
78. Fry, L.; Bowlin, A.; Roys, H.; Weinkopff, T. Distinct Lymphatic Remodeling Is Associated with Healing and Non-Healing Murine Cutaneous Leishmaniasis. *J. Immunol.* **2023**, *210*, 81.07. [CrossRef]